



Spatial variation, source identification, and quality assessment of surface water geochemical composition in the Indus River Basin, Pakistan

Faizan Ur Rehman Qaisar^{1,2,3,4,5} · Fan Zhang^{1,2,3,4}  · Ramesh Raj Pant^{1,2,3,4,6} · Guanxing Wang^{1,2,3,4} · Sardar Khan⁷ · Chen Zeng^{1,2}

Received: 8 November 2017 / Accepted: 8 February 2018 / Published online: 22 February 2018
© Springer-Verlag GmbH Germany, part of Springer Nature 2018

Abstract

The Indus River Basin (IRB) with an area of 139,202 km² is the lifeline river basin of Pakistan. An intensive study was conducted in six subcatchments of the IRB with five in the Upper Indus Basin (UIB) and one of the Lower Indus Basin (LIB; between Tarbela Dam and Panjand), i.e., the Gilgit River Basin (UIB-I), Hunza River Basin (UIB-II), UIB-III, UIB-IV and UIB-V, and LIB. A total of 84 surface water samples were collected from main stream and tributaries from June to August, 2016. The pH, electric conductivity (EC), and total dissolved solids (TDS) were measured in situ, whereas major ions (Ca²⁺, Mg²⁺, K⁺, Na⁺, Cl⁻, SO₄²⁻, and NO₃⁻) and Si were analyzed in the laboratory. The results exhibited alkaline pH (8.55 ± 0.20) with diverse TDS (114.69 ± 77.65 mg L⁻¹) and ion concentrations that were characterized primarily by the Ca-Mg-HCO₃ type in the whole basin. The average TDS in the UIB and LIB were 93.99 ± 39.73 and 181.67 ± 167.82 mg L⁻¹, respectively, under the influence of the arid to semi-arid climatic conditions and relatively higher anthropogenic interference in LIB compared to the UIB. The order of dominant major cations was different in the UIB and LIB, reflecting the diverse nature of geological formation. Gibbs plot, mixing diagrams, and ionic ratios were used to identify the controlling mechanism of river geochemistry in the IRB as carbonate weathering in general with different degrees of silicate weathering and minor contribution by evaporite dissolution. In addition, principal component/factor analysis also indicated that the major sources of dissolved loads in the basin are carbonates followed by silicates. Significant influences of silicate minerals were observed in the LIB, and there was a large contribution of evaporites in the UIB-II, UIB-III, and LIB. The suitability assessment showed that the river water fits the WHO permissible limits for drinking purposes from the perspective of major ions, whereas for irrigation purposes, most of the samples exhibited excellent and good levels except for a couple of permissible and doubtful levels from the Sawan and Deratang tributaries in the LIB, which may deteriorate the quality of soil and degrade the water quality downstream.

Keywords Indus River Basin · Geochemistry · Spatial variation · Source identification · Controlling factors · Water quality

Responsible editor: Philippe Garrigues

Electronic supplementary material The online version of this article (<https://doi.org/10.1007/s11356-018-1519-z>) contains supplementary material, which is available to authorized users.

✉ Fan Zhang
zhangfan@itpcas.ac.cn

¹ Key Laboratory of Tibetan Environment Changes and Land Surface Processes, Institute of Tibetan Plateau Research, Chinese Academy of Sciences, Beijing, China

² Key Laboratory of Alpine Ecology and Biodiversity, Institute of Tibetan Plateau Research, Chinese Academy of Sciences, Beijing, China

³ CAS Center for Excellence in Tibetan Plateau Earth Sciences, Beijing, China

⁴ University of Chinese Academy of Sciences, Beijing, China

⁵ Department of Earth Sciences COMSATS Institute of Information Technology, Abbottabad, Pakistan

⁶ Central Department of Environmental Science, Tribhuvan University, Kirtipur, Nepal

⁷ Department of Environmental Sciences, University of Peshawar, Peshawar, Pakistan

Introduction

The water quantity and quality of the Himalaya are among the most important and sensitive issues worldwide from the view of human well-being and ecological integrity (Barnett et al. 2005; Vörösmarty et al. 2010). The bedrock in the Himalaya is subjected to high weathering rates under the extreme climate conditions (Ali and De Boer 2007). Despite the fact that only 4% of the global land surface has been secured by the Himalaya, 25% of total dissolve loads entering into the oceans has been generated from the region (Raymo and Ruddiman 1992). Recent investigations of the Himalayan regions that focus on hydrochemical characteristics have revealed that surface water quality has been deteriorating in the past few decades due to rise in temperature, variable precipitation, poor land use, urbanization, deforestation, and mineral resources exploitation (Sun et al. 2012; Wu et al. 2012). Notably, the rivers and their tributaries that pass through the cities in the developing countries of South Asia such as Pakistan, Nepal, India, and Bangladesh receive large amount of contaminants released from industrial, domestic/sewage, and agricultural effluents (Karn and Harada 2001; Kambole 2003; Pekey et al. 2004; Richardson et al. 2015).

Investigations of river basins provide unique insights into the hydrologic functions of the individual parts of the catchment, because the geochemistry of rivers is regulated by complex interactions among various physical, chemical, and biological environments (Brezonik and Arnold 2011; Stumm and Morgan 2012). The notable studies on source identification and controlling factor of rivers worldwide are underscored as those of the Amazon (Stallard and Edmond 1987), the Upper Yangtze (Chen et al. 2002), the Mississippi (Battaglin et al. 2001), the Yenisei (Kimstach et al. 1998), the Yellow (Chen et al. 2005), and the Ganga and Yamuna Rivers (Dalai et al. 2002) and have stated that the major drivers of hydrochemical characteristics are climate, lithology, hydrology, and anthropogenic interferences (Gibbs 1970; Meybeck 1987; Qadir et al. 2008).

A basin-wise study was performed on weathering processes in the Indus River Basin (IRB) of Pakistan with a focus on carbon, sulfur, oxygen, and strontium isotopes (Karim and Veizer 2000). Some of the major tributaries of the IRB were studied by Subramanian (1979) and Pande et al. (1994) at a provincial level from India to Karachi in Pakistan. These studies used elemental and isotopic data and proposed that carbonate weathering and evaporite dissolution were controlling factors. Jacobson and Blum (2000) used major ions and strontium isotopes to determine disseminated calcite in Himalayan silicate rocks in order to evaluate the consumption of CO₂ from the atmosphere. A subsequent geochemical study was reported by Qadir et al. (2008) in the Chenab River in which the spatiotemporal variations of water quality were explored. Apart from these studies, the water

quality parameters in the Jamshoro area of Pakistan was evaluated by Baig et al. (2009), who found that Na⁺, K⁺, and SO₄²⁻ concentrations were elevated because of the semi-arid environment and anthropogenic interferences.

The headwater areas in the Third Pole have been considered as one of the most pristine regions in the world (Paudyal et al. 2016). However, some recent studies indicated that South Asian regions with heavy pollution could be the source of contaminations, which could be long range transported to the remote Himalayan regions and deposited via wet and dry deposition through atmospheric circulations in the regions (Tripathee et al. 2014, 2016b).

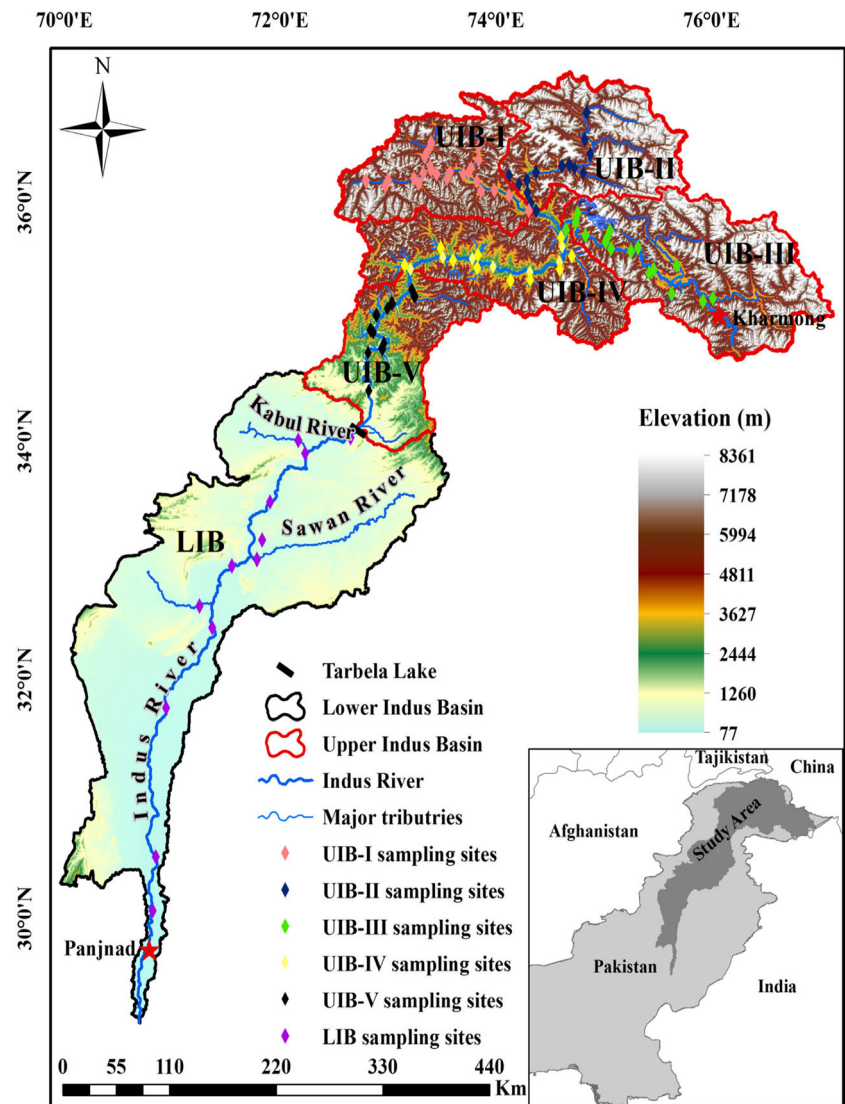
It is noted from previous literatures that changing climatic conditions promote accelerated hydrochemical dynamics. In addition to the climate and lithology, as well as land use conditions, the IRB is also characterized with partial anthropogenic signatures, particularly in the downstream segment. Systematic studies on geochemical variabilities and implication of natural and anthropogenic factors are imperative to elucidate and protect the water quality in the basin. However, there are very limited published data available, which represent a significant research gap in understanding the geochemistry of the river. Therefore, the objective of this study is to evaluate the spatial variation of hydrochemical attributes, their sources, and controlling factors in the IRB. Since the basin is the lifeline of Pakistan and fundamentally supports economic activities, the suitability of the river water for human consumptions and irrigation purposes was also assessed.

Materials and methods

Study area

The Indus River originates from Lake Mansarovar in Tibetan Plateau, enters India, then flows through Pakistan, and finally empties into the Arabian Sea (Tahir et al. 2016). The IRB is located between latitudes 29° 30' N and 37° 10' N and between longitudes 70° 15' E and 77° 0' E, covering a total area of 139,202 km² (with 8, 39, and 53% in China, India, and Pakistan, respectively). The area is confined between Kharmonj and Panjnad, which is the confluence point of the Indus River with other rivers of Pakistan (Fig. 1). On the basis of climate, geology, land use, and topography, the IRB is classified into the Upper Indus Basin (UIB) (54%) and Lower Indus Basin (LIB) (46%), which are separated by the Tarbela Dam, situated at an elevation of 440 m (Ali and De Boer 2007) (Fig. 1). The LIB specified in this study is actually the mid-stream part of the whole IRB. The UIB lies between 440 and 8361 m asl, is mainly affected by westerlies, and is principally fed by glacier/snow melt (Liniger et al. 1998; Hewitt 2005). In contrast, the LIB lies between 70 and

Fig. 1 Map of the Indus River Basin, its divisions, and major tributaries



440 m asl and is mostly characterized by an arid to semi-arid climate (Fig. A1), in which flow is primarily controlled by discharge from upstream, tributaries, and monsoon precipitation. The mean annual precipitation and air temperature range between 200 and 1400 mm and between 5 and 20 °C, respectively, in the UIB and between 200 and 1200 mm and between 10 and 32 °C, respectively, in the LIB, showing distinct differences between upper and lower segments (Baloch et al. 2006; Liu et al. 2012; Nadeem Faisal 2015; Lutz et al. 2016).

The UIB extends over parts of the Hindukush, Karakoram, and Western Himalayan ranges and is subjected to different microclimate regimes (Young and Hewitt 1990; Dimri and Chevuturi 2014). Within the UIB, the Gilgit (UIB-I) and Hunza (UIB-II) River basins are considered separately for detailed study because they are the largest subcatchments of the IRB. UIB-I originates in the Hindukush region, where the flow mostly depends upon rainfall (westerlies) and melt water (Hewitt 2005; Tahir et al. 2011). UIB-II originates near Khunjrab and

then passes and flows through the center of the Karakoram ranges, where a substantial proportion of the flow is derived from glacial melt. The remainder of the UIB is further divided into three subcatchments in this study on the basis of their sources (UIB-III from glacial melt, UIB-IV from snowmelt, and UIB-V mostly from monsoonal precipitation). Maximum annual precipitation was observed at UIB-V and the northern part of LIB, whereas other parts of the investigation territory have low annual precipitation (Fig. A1). The land use of the IRB is classified into eight major classes, including water bodies, forests, shrublands, grasslands, agricultural areas, built-up area, snow/glaciers, and barren areas (Loveland et al. 2000). From north to south, the IRB is geologically split into five lithotectonic divisions (Fig. A2): (1) the Hindu Kush–Karakoram–Western Tibet Block (HKT), (2) the Kohistan–Ladakh Arcs (KLA), (3) the Higher Himalayas (HH), (4) the Lesser Himalayas and the Foothills (LHF), and (5) the Southern Sedimentary Basin (SSB) (Karim and Veizer 2000). Each division accommodates different rock formations,

which contributes to the variety of dissolved loads in surface and groundwater. The details of the land use and geological formations of the IRB are explained in the supplementary file (Figs. A1 and A2).

Sampling and laboratory analysis

Water samples were collected from main stream and tributaries at 84 different sites (Fig. 1) throughout the IRB from June to August, 2016. Considering the diversity in climate, geology, land use, and anthropogenic activities, 17, 14, 15, 17, 10, and 11 water samples were collected from UIB-I, UIB-II, UIB-III, UIB-IV, UIB-V, and the LIB, respectively (Table A1), following the standard guideline values (APHA 2005; Duncan et al. 2007). For both the main stream and tributaries, three water samples were collected from each sampling site at depth of ≈ 30 cm beneath the surface (two from each bank and one from the center) and were thoroughly mixed. pH, electric conductivity (EC), total dissolved solids (TDS), and water temperature (Tem.) were measured on-site by using an Oakton PCSTestr 35. Samples were instantly filtered through a 0.45- μm polytetrafluoroethylene (PTFE) disk syringe filter and filled in high-density polyethylene (HDPE) bottles of 30 mL.

The concentrations of the major cations (Ca^{2+} , Mg^{2+} , Na^+ , K^+) and Si were determined by inductively coupled plasma optical emission spectrometry (ICP-OES, Optima 5300 DV, PerkinElmer, Waltham, MA, USA) with a limit of detection of 0.01 mg L^{-1} , and major anions (Cl^- , NO_3^- , and SO_4^-) were determined using ion chromatography (ICS-2500, Thermo Fisher Scientific, Waltham, MA, USA) with LOD of 0.01 mg L^{-1} (Li et al. 2015; Tian et al. 2016) at the Institute of Tibetan Plateau Research, Chinese Academy of Sciences. Special care was taken during the sampling and laboratory analysis. All of the sample bottles were soaked overnight in 15% HCl and washed with deionized water before using in order to remove potential contaminants introduced during packing and shipping (APHA 2005). The sample bottles were sealed by using Parafilm and stored below 4°C until laboratory analysis. Distilled deionized water was used to clean the equipment after every sample measurement on site. External standards for major cations and anions were prepared from the national standard solutions obtained from the Certified Reference Material Center, China (Tian et al. 2016).

For quality control and quality assurance, the standard operating procedures were strictly followed during sampling and laboratory analysis as directed by APHA (2005). In order to avoid contamination, powder-free nitrile exam gloves and mask was used during the sample collection and testing. At each sampling site, three water samples, i.e., at left bank, middle, and right bank of the river, were taken and mixed before a composite sample was prepared. The sample bottles were rinsed three times with the same water before the final sample

was acquired. Before the in situ measurements, the instruments were properly calibrated. Triplicate samples were run, and the average recovery of quality control analysis was $99 \pm 4\%$, indicating the good quality of the data. In addition, four blank samples of deionized water filtered through 0.45- μm polytetrafluoroethylene (PTFE) disk syringe filter, filled in high-density polyethylene (HDPE) bottles, sealed with Parafilm were collected in the field and kept in the same environment with other water samples. The results of these field blank samples showed negligible contamination during the sampling, filtering, and storage processes, as the values of most hydrochemical variables were below the detection limit (Paudyal et al. 2016). The average analytical precision for both cations and anions was better than 2%. The alkalinity as HCO_3^- was estimated by charge balance (Li et al. 2016). To verify the accuracy, sums of major ions were calculated and compared to the TDS values ($\Sigma\text{ions} = 1.06 \text{ TDS}$, $r = 0.97$), which illustrated highly acceptable data quality (Tripathee et al. 2014; Paudyal et al. 2016; Pant et al. 2018).

To interpret the data and develop a conclusive understanding of the geochemistry of the IRB, a series of statistical tests were performed using an IBM SPSS 22.0 (Xiao et al. 2012; Pant et al. 2018). These tests include a normality test, descriptive statistics (mean, max, min, SD etc.), Spearman correlation, and principal component analysis and factor analysis (PCA/FA) (Varol et al. 2013a). The normality test and correlation analysis were performed by considering all of the parameters to predict the degree of dependent of one variable on others with a correlation significance level of 0.01. PCA/FA was applied to group the changing patterns of major ions in order to explain the fluctuation in dataset with minimum loss of original information. PCA/FA is attained by analyzing the correlation matrix and transforming the original variables to uncorrelated ones, commonly called varifactors (VFs) (Helena et al. 2000). Additionally, the eigenvalues in PCA/FA define how much variance is present in associated VFs. The VF that holds the maximum eigenvalue is found to have the most covariability (Tripathee et al. 2016a). Suitability of the dataset for PCA/FA was tested by using the Kaiser–Meyer–Olkin (KMO) and Bartlett’s sphericity methods which is run prior to PCA/FA. Furthermore, Gibbs, Piper, mixing diagrams, and ionic ratios were used for source identification and controlling factor analysis. The sodium ion percentage and sodium absorption ratio (SAR) were used to evaluate the irrigation water quality (Wilcox 1948; Richards 1954; Bauder et al. 2011; Thomas et al. 2014).

Results and discussion

General geochemical characterizations

The descriptive statistics of major geochemical variables of the IRB and comparison with other river basins in the surrounding

Table 1 Summary statistics of geochemical compositions of the IRB and a comparison to other rivers in the region

River	P	EC	TDS	pH	Ca ²⁺	Mg ²⁺	K ⁺	Na ⁺	Si	Cl ⁻	NO ₃ ⁻	SO ₄ ²⁻	HCO ₃ ⁻	Reference
<i>Indus River Basin,</i>	Mean/median	158.5 ^c	114.69 ^c	8.55 ^c	20.69 ^a	3.77 ^c	3.56 ^b	5.21 ^b	1.79 ^c	3.06 ^b	1.86 ^c	18.53 ^c	60.41 ^c	This study
<i>Pakistan</i>	SD	105.24	77.65	0.2	8.86	3.79	2.64	16.36	1.13	15.6	1.56	15.5	38.42	
Jhelum River, Pakistan	842	349	440	7	55	45	8.1	37		44	–	–	22	Iqbal et al. (2017)
Chenab River, Pakistan	1250–1875	–	148.5	8.09	12.8	1.96	3.2	5.37	1.53	1.78	2.74	8	68.63	Karim and Veizer (2000), Ashouri et al. (2015)
Ravi River, Pakistan	870–1000	–	179.6	8.09	15.05	2.34	3.63	10.92	2.32	4.45	3.31	7.99	100.95	Karim and Veizer (2000), Ashouri et al. (2015)
Yarlung Tsangpo, China	443.51	249	117.3	8.8	27.9	5.1	1	5.7	–	2.39	1	37.4	74.1	Li et al. (2011), Qu et al. (2017)
Upper Yangtze River, China	625–750	–	778	7.98	53.4	22.9	5.5	157.7	–	233.7	1.3	114.9	188.5	Ashouri et al. (2015)
Upper Mekong, China	300–600	–	302	8.42	49	14	1	12	1.86	14	–	69	138	Kiem et al. (2008), Huang et al. (2009)
<i>Global mean</i>	–	–	120	8	15	4.1	2.3	6.3	7.63	7.8	1	11.2	58.4	Gaillardet et al. (1999), Meybeck (2003)
<i>WHO limit</i>	–	–	1000	6–8	100	50	100	200	–	250	50	250	600	WHO (2011)

All units in milligram per liter except P (mm), pH, and EC (μS cm⁻¹)

SD standard deviation, P annual precipitation extracted from TRMM monthly data product of 2012–2016 (Liu et al. 2012)

^a Arithmetic mean for normal distribution

^b Geometric mean for log-transformed normal distribution

^c Median value for non-normal distribution

region are summarized in Table 1. Arithmetic mean values, geometric mean values, and median values were used for normally distributed datasets, log-transformed normally distributed datasets, and non-normally distributed datasets, respectively (Wang et al. 2017).

The pH of the IRB was found to be alkaline in nature (8.57 ± 0.20) and higher than the global mean (i.e., 8), which revealed the potential impact of carbonate-dominated lithologies in the basin (Li and Zhang 2008; Zhang et al. 2009). The degree of mineralization process in the basin is indicated by EC and TDS, which exhibited substantial variations with high standard deviations ($158.5 \pm 105.24 \mu\text{S cm}^{-1}$ and $114.69 \pm 77.64 \text{ mg L}^{-1}$, respectively). The higher TDS values in the IRB than that of the global mean values for the large rivers (i.e., 120 mg L^{-1}) could be attributed to lithoclimatic settings and anthropogenic interferences in the basin (Jonnalagadda and Mhere 2001). The grand mean concentrations of TDS in the IRB were comparable to that of the Yarlung Tsangpo River in Tibet and global mean value, but were markedly lower than those of the other rivers in Pakistan and Tibet (Table 1).

Calcium ($20.68 \pm 8.86 \text{ mg L}^{-1}$) was the most abundant major cation in the basin followed by sodium ($5.21 \pm 16.36 \text{ mg L}^{-1}$), magnesium ($3.77 \pm 3.79 \text{ mg L}^{-1}$), and potassium ($3.56 \pm 2.64 \text{ mg L}^{-1}$), and Na^+ had the most significant variation. Bicarbonate ($60.41 \pm 38.41 \text{ mg L}^{-1}$) was the most dominant major anion in the basin followed by sulfate ($18.53 \pm 15.50 \text{ mg L}^{-1}$), chloride ($6.06 \pm 15.60 \text{ mg L}^{-1}$), and nitrate ($1.46 \pm 1.56 \text{ mg L}^{-1}$), and Cl^- had the most significant variation. The large variation in Na^+ and Cl^- concentrations could be attributed to multiple geogenic and anthropogenic sources (Tian et al. 2016). The concentrations of major ions in the IRB were more comparable than those of the Yarlung Tsangpo River and global mean values than to those of other rivers in surrounding regions (Table 1). However, the mean concentration of silica was found to be $1.79 \pm 1.13 \text{ mg L}^{-1}$, which was less than the global mean (7.63 mg L^{-1}), indicating less intense silicate weathering in the IRB. The mean concentration of NO_3^- approximately two times that of the global mean and other rivers in the surrounding region, indicating possible enrichment from anthropogenic activities (Meybeck 2003; Wang et al. 2006; Liu et al. 2015). In summary, the major ionic concentrations of the IRB are within the range of WHO limits, and mostly comparable to the global mean values of the world's major rivers (Table 1).

Spatial patterns of major ions

The descriptive statistics of major geochemical attributes at the subcatchment level in the IRB are shown in Table 2 and Fig. A3. The mean pH values of all subcatchments were alkaline and did not differ much. However, EC and TDS displayed a considerable

variability. Elevated mean concentrations of TDS in the LIB ($181.67 \pm 167.82 \text{ mg L}^{-1}$) compared to the UIB ($93.99 \pm 39.73 \text{ mg L}^{-1}$) were chiefly ascribed to the arid to semi-arid climatic conditions and higher anthropogenic interferences supported by land use variations (Fig. 2) (Gburek and Folmar 1999; Dalai et al. 2002; Chen et al. 2005). Remarkable differences exist in the relative abundance of cations in the UIB and LIB samples, in which cations in the UIB samples follow the order of $\text{Ca}^{2+} > \text{Mg}^{2+} > \text{K}^+ > \text{Na}^+$ and cations in the LIB water samples follow the order of $\text{Ca}^{2+} > \text{Na}^+ > \text{Mg}^{2+} > \text{K}^+$. The concentrations of all of the ions were remarkably higher in the LIB. Specifically, the Na^+ and Cl^- concentrations were ~ 10 -fold higher than those in the UIB, which can be explained by the semi-arid environment, local sources of halite, and intensive anthropogenic interferences, particularly agricultural practices (Xiao et al. 2012). Remarkably higher concentrations of NO_3^- were observed in the LIB, which is characterized by intensive agriculture activities. Additionally, there is a strong correlation in the UIB between Ca^{2+} - Mg^{2+} ($r = 0.83$), Ca^{2+} - HCO_3^- ($r = 0.87$), and Mg^{2+} - HCO_3^- ($r = 0.91$), whereas there is not a strong correlation between the aforementioned pairs in the LIB (Table A2), indicating the dominance carbonate weathering in the UIB (Varol et al. 2013b; Shammi et al. 2017).

Within UIB, the two glaciated subcatchment, i.e., UIB-II and UIB-III, illustrated higher TDS, indicating the high weathering rate in glaciated areas (Brown et al. 1996) and dilution by snowmelt and precipitation in UIB-I, UIB-IV, and UIB-V. Most of the major ions showed similar spatial patterns within UIB corresponding with the TDS values. For example, UIB-II and UIB-III represented higher SO_4^{2-} contents than UIB-I, UIB-IV, and UIB-V indicating greater rock-water interaction time with pyrite dissolution. In contrast, LIB, UIB-IV, and UIB-V have higher Si concentrations compared with UIB-I, UIB-II, and UIB-III, indicating potential dissolution of silicate minerals from pedogenic processes (Reynolds and Johnson 1972; Xiao et al. 2015).

A strong positive correlation was observed between Ca^{2+} - SO_4^{2-} ($r = 0.83, 0.74, 0.73, 0.91, \text{ and } 0.80$ for UIB-I, UIB-II, UIB-III, UIB-IV, and LIB, respectively) and Mg^{2+} - SO_4^{2-} pairs ($r = 0.88, 0.66, 0.61, \text{ and } 0.65$ for UIB-I, UIB-II, UIB-IV, and LIB, respectively) (Table A2) indicating sulfate mineral dissolution and oxidation of pyrites as the common source of SO_4^{2-} in the subcatchments (Xiao et al. 2015). In UIB-I, there was strong positive correlation between NO_3^- - Ca^{2+} , NO_3^- - Mg^{2+} , and NO_3^- - Na^+ pairs ($r = 0.66, 0.70, \text{ and } 0.72$, respectively), which could be resulted from the use of chemical fertilizers and leaching of soil salts due to intensive agricultural practices (Butz 1989; Sharma et al. 2012; Chen et al. 2015). In addition, the higher NO_3^- values in UIB-V also indicate more intensive anthropogenic activities supported

Table 2 Summary statistics of spatial patterns of hydrogeochemical attributes in the IRB

Location		P	RD	pH	TDS	Ca ²⁺	Mg ²⁺	K ⁺	Na ⁺	Si	Cl ⁻	NO ₃ ⁻	SO ₄ ²⁻	HCO ₃
UIB-I (n = 17)	Mean/median	301 ^a	803 ^a	8.65 ^a	103.13 ^a	18.12 ^a	4.81 ^b	1.57 ^a	1.47 ^a	1.76 ^a	1.94 ^b	1.72 ^b	17.99 ^a	58.3 ^b
	SD	24	184	0.24	40.76	7.61	3.63	0.63	0.67	0.26	1.67	0.68	8.76	32.7
UIB-II (n = 14)	Mean/median	273 ^a	705 ^a	8.62 ^a	165.01 ^c	27.333 ^c	6.9 ^a	4.94 ^b	3.08 ^c	1.46 ^c	1.32 ^a	1.25 ^a	40.38 ^c	77.88 ^a
	SD	58	81	0.18	40.81	6.25	3.50	3.07	1.10	0.36	0.73	0.43	15.78	24.5
UIB-III (n = 15)	Mean/median	270 ^a	1973 ^a	8.59 ^a	121.87 ^a	21.43 ^a	3.51 ^a	2.7 ^a	2.53 ^c	1.73 ^a	2.06 ^c	1.19 ^a	22.28 ^a	58.28 ^a
	SD	43.48	464	0.16	28.45	6.13	2.54	1.23	1.83	0.29	1.54	0.48	10.99	19.85
UIB-IV (n = 17)	Mean/median	408 ^a	821 ^a	8.51 ^a	106.04 ^c	19.83 ^c	1.67 ^c	2.03 ^a	2.10 ^a	1.80 ^c	1.93 ^b	1.72 ^b	14.07 ^a	42.2 ^a
	SD	131	183	0.18	36.58	7.62	1.43	1.04	1.07	0.36	1.17	0.55	10.51	19.26
UIB-V (n = 10)	Mean/median	908 ^a	499 ^a	8.54 ^a	83.01 ^a	16.25 ^a	2.52 ^a	2.42 ^a	2.54 ^b	2.01 ^c	2.49 ^a	2.39 ^a	15.42 ^c	48.2 ^a
	SD	294.21	105	0.21	38.77	7.74	1.41	1.27	2.02	1.29	1.5	1.15	6.23	25.36
Whole UIB (n = 73)	Mean/median	432 ^a	1053 ^a	8.55 ^b	93.99 ^a	17.81 ^a	3.53 ^c	2.36 ^b	2.10 ^c	1.74 ^c	2.15 ^b	1.37 ^c	17.12 ^c	49.40 ^a
	SD	110	437	0.18	39.73	7.5	1.96	1.18	1.6	0.71	1.39	0.83	10.59	21.7
Whole LIB (n = 11)	Mean/median	650 ^a	136 ^a	8.49 ^a	181.67 ^b	24.27 ^c	8.08 ^b	5.98 ^b	22.69 ^b	4.47 ^b	22.15 ^b	4.28 ^a	36.86 ^a	114.9 ^a
	SD	241	486	0.23	167.82	10.64	5.53	4.42	41.03	2.12	40.16	3.04	22.67	60.64

All units in milligrams per liter except P (mm), RD (mm), pH, and EC (μS cm⁻¹). RD > P indicates additional water supply from melt water, and RD < P reflects excess use of water for agricultural practices

SD standard deviation, P annual precipitation extracted from TRMM monthly data product of 2012–2016 (Liu et al. 2012), RD runoff depth calculated based on available data of discharge measured at different seasons (2003–2007) of the river reach divided by the corresponding catchment area

^a Arithmetic mean for normal distribution

^b Geometric mean for log-transformed normal distribution

^c Median value for non-normal distribution

by land use characteristics as compared with other subcatchments of the UIB (Fig. A1).

Characterization of geochemical facies

Major cations and anions (milli-equivalent %) are plotted in a Piper diagram (Fig. 2), in which the cations and anions are illustrated in the bottom left and right triangles, respectively, and are further projected into the central diamond field to evaluate geochemical facies (Piper 1944). In the cation triangle, most of the samples lie in the left corner where Ca²⁺ values are higher (> 50%), revealing the dominance of calcium. Two samples from the LIB lie towards the right corner of the cation plot, displaying an increased concentration of sodium and potassium ions, which indicates the influence of local sources of Na⁺ and K⁺ (Karim and Veizer 2000; Selemeni et al. 2017). In contrast, in the anion triangle, most of the samples lie on the left side of the triangle, showing a dominance of HCO₃⁻ over Cl⁻ and SO₄²⁻. However, two samples from the LIB and one sample each from UIB-III, UIB IV, and the LIB showed higher concentrations of Cl⁻ and SO₄²⁻, which could be due to the mixed sources of multiple geogenic and anthropogenic activities (Xiao et al. 2012). There are six subfields in the diamond-shaped Piper diagram (Fig. 2): (1) Ca Mg-HCO₃, (2) Na Cl, (3) mixed Ca Mg Cl, (4) mixed Ca Na HCO₃, (5) Ca SO₄-Cl, and (6) Na HCO₃ (Manoj et al. 2013). Mostly, the geochemical facies of the IRB are characterized by the Ca-Mg-HCO₃⁻ type (91.6%). Apart from this, two samples from UIB-I, one sample from UIB-III, and two samples from LIB are the Ca-Na-HCO₃⁻ type. All of

these samples were taken from river reaches with relatively low discharge, or more anthropogenic activities. Only one sample lies in the Na-Cl type (LIB: Deratang tributary), and one lies in the Ca-SO₄-Cl type (UIB-IV: Jaglot tributary). The Jaglot tributary was influenced by pyrite deposits and mining activities, whereas the Deratang tributary is recognized to have halite deposit within the sedimentary rocks as well as sewage waste from nearby urban land use. The hydrochemical facies clearly suggested spatial discrimination among different subcatchments with anthropogenic and geogenic signatures.

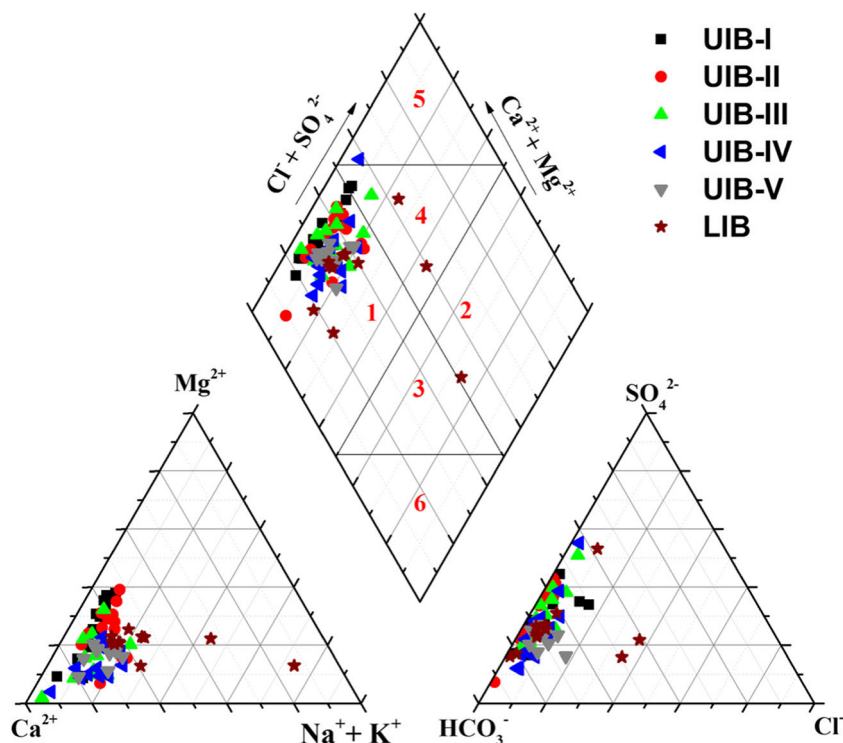
Mechanisms controlling the major ion chemistry of the IRB

Major ions of river water have multiple sources from physical, chemical, and biological processes in the basin, including the sea salts that are carried by atmosphere circulation and are deposited through precipitation, weathering of different types of rocks such as carbonates, silicates, and evaporites, and anthropogenic activities (Patz et al. 2005; Zhang et al. 2007).

Gibbs plot

Surface water chemistry and its controlling mechanisms were well defined by Gibbs (1970). The Gibbs plot (Fig. 3) explained three end-members: precipitation, rock dominance, and evaporation from bottom to top. In general, samples with low TDS (≈ 10.0 mg L⁻¹) and high Na⁺/(Na⁺ + Ca²⁺) and Cl⁻/(Cl⁻ + HCO₃⁻) (≈ 1.0) fall on the lower right corner, which reflects the influence of precipitation. Samples with medium

Fig. 2 Piper diagram showing the hydrochemical facies of the Indus River Basin



amount of dissolved salts ($70.0\text{--}300.0\text{ mg L}^{-1}$) with $\text{Na}^+(\text{Na}^+ + \text{Ca}^{2+})$ and $\text{Cl}^-(\text{Cl}^- + \text{HCO}_3^-)$ ratios < 0.5 are located on the middle left side of the plot near the rock dominance end-member. When the TDS increases above 300.0 mg L^{-1} and the ratio of $\text{Na}^+(\text{Na}^+ + \text{Ca}^{2+})$ or $\text{Cl}^-(\text{Cl}^- + \text{HCO}_3^-)$ ratios approaches 1.0, evapocrystallization is dominant (Stallard and Edmond 1987). Figure 3 reveals that most of the water samples from the IRB were dominated by rock weathering. Two samples from the LIB lie towards the evaporation end-member, indicating the impact of arid to semi-arid environmental conditions.

Mixing diagram

Different combinations of major ions can result from weathering of different rocks. For instance, carbonate weathering produces Ca^{2+} , Mg^{2+} , and HCO_3^- , silicate weathering generates Na^+ , K^+ , Si , Ca^{2+} , Mg^{2+} , and HCO_3^- , and dissolution of evaporites or leaching of soil salts mainly produces SO_4^{2-} , Ca^{2+} , Mg^{2+} , Na^+ , K^+ , Cl^- , and NO_3^- (Karim and Veizer 2000; Dalai et al. 2002; Han and Liu 2004; Zhang et al. 2007). In addition, Na^+ , Cl^- , and SO_4^{2-} also occur from the dissolution of halite, pyrite, and sulfate minerals such as gypsum and anhydrite (Qadir et al. 2008; Paudyal et al. 2016). To show the origins of the riverine dissolved load produced by chemical weathering in a basin with complex lithologies, Na^+ -normalized molar ratios were plotted in the mixing diagram (Fig. 4) with respect to three representative lithologies (Gaillardet et al. 1999). The results clearly show that the

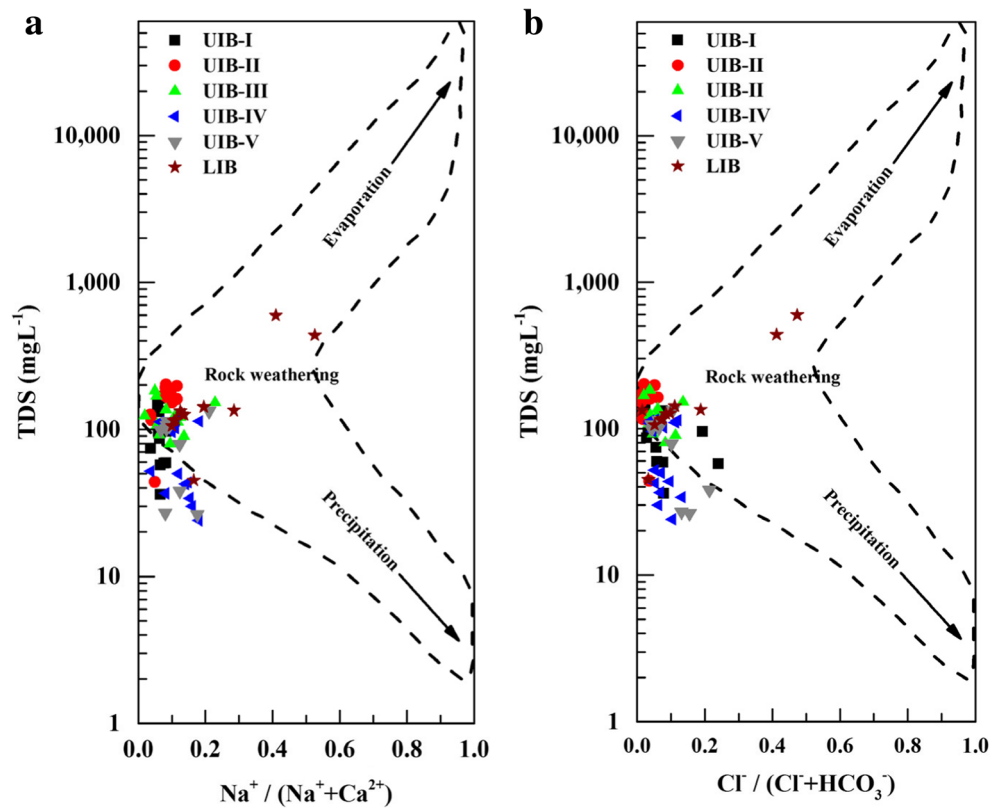
majority of the IRB surface waters were dominated by carbonate weathering with influences of silicate weathering to different degrees and a minor contribution of evaporite weathering. Carbonate weathering is the controlling factor ($> 90\%$) for the major dissolved load in UIB-I and UIB-II, as shown by the samples that were close to the end-member of carbonate. Mixing of carbonate ($> 50\%$) and silicate weathering in UIB-II, UIB-IV, and UIB-V can be inferred from the parallel trend line between two end-members of these minerals, whereas the larger influence of silicate minerals was observed in the LIB based on samples near the silicate end-member. Slight shifting from the line between the carbonate and silicate end-members towards the evaporite end-member indicated a minor contribution by evaporite dissolution, especially in UIB-III, UIB-IV, UIB-V, and the LIB.

Ionic ratios

The sources of Ca^{2+} , Mg^{2+} , and HCO_3^- can be determined from the $\text{Ca}^{2+} + \text{Mg}^{2+}/\text{HCO}_3^-$ ratio (Fig. 5a). Almost all the samples lie close to the 1:1 line, indicating that the controlling mechanism of Ca^{2+} , Mg^{2+} , and HCO_3^- is carbonate weathering (Varol et al. 2013b). The high correlation between Ca^{2+} and Mg^{2+} (Fig. 5b) clearly indicated that both ions are mostly from same source region (Zhang et al. 2007).

A plot of $\text{Na}^+ + \text{K}^+$ vs. Si (Fig. 5c) revealed an increasing trend of Si with respect to $\text{Na}^+ + \text{K}^+$ in the LIB indicating silicate weathering from clastic sedimentary rocks. However, clustered data points of the UIB samples revealed

Fig. 3 Ratios of **a** $\text{Na}^+ / (\text{Na}^+ + \text{Ca}^{2+})$ and **b** $\text{Cl}^- / (\text{Cl}^- + \text{HCO}_3^-)$, as a function of TDS



relatively less favorable conditions for dissolving silica. The mean $\text{Si} / (\text{Na}^+ + \text{K}^+)$ ratio in UIB-I, UIB-II, UIB-III, UIB-IV, UIB-V, and the LIB was 0.70, 0.27, 0.53, 0.62, 0.58, and 0.21, respectively, indicating less intensive silicate weathering and

additional input of Na^+ and K^+ from multiple sources (Na-bearing salts and anthropogenic activities), particularly in the LIB.

The $\text{Ca}^{2+} + \text{Mg}^{2+} / \text{Na}^+ + \text{K}^+$ ratio (Fig. 5d) is widely used to evaluate the relative contribution of different types of rock in a

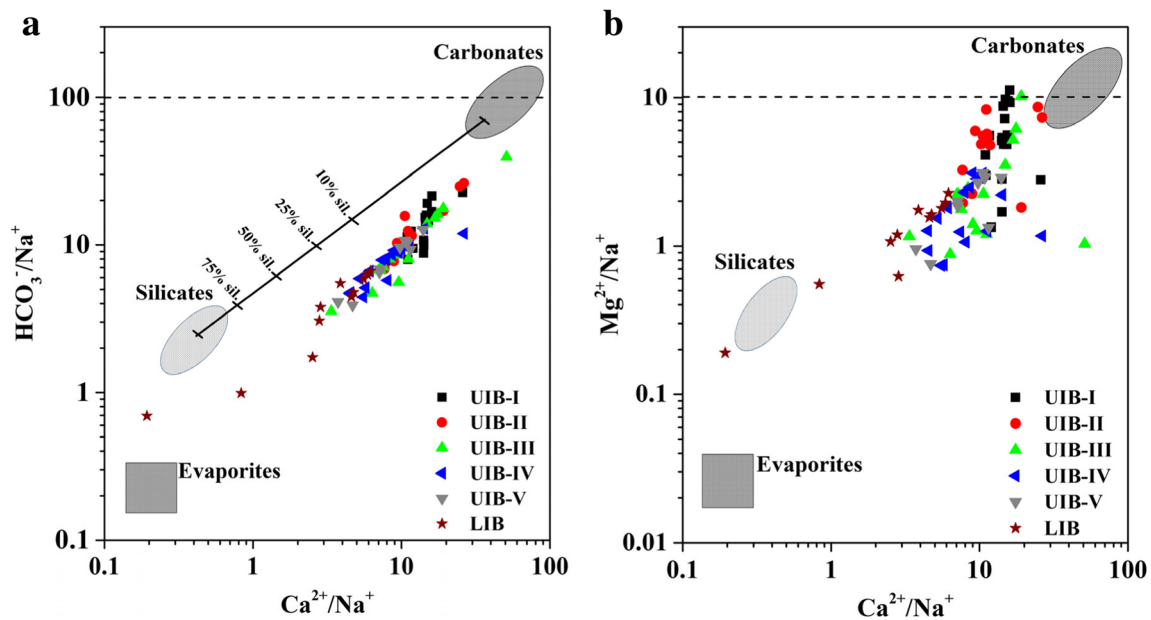


Fig. 4 **a** Mixing diagram of Na^+ -normalized Ca^{2+} vs. HCO_3^- with background information obtained from Moon et al. (2009). **b** Mixing diagram of Na^+ -normalized Ca^{2+} vs. Mg^{2+} with background information obtained from Gaillardet et al. (1999)

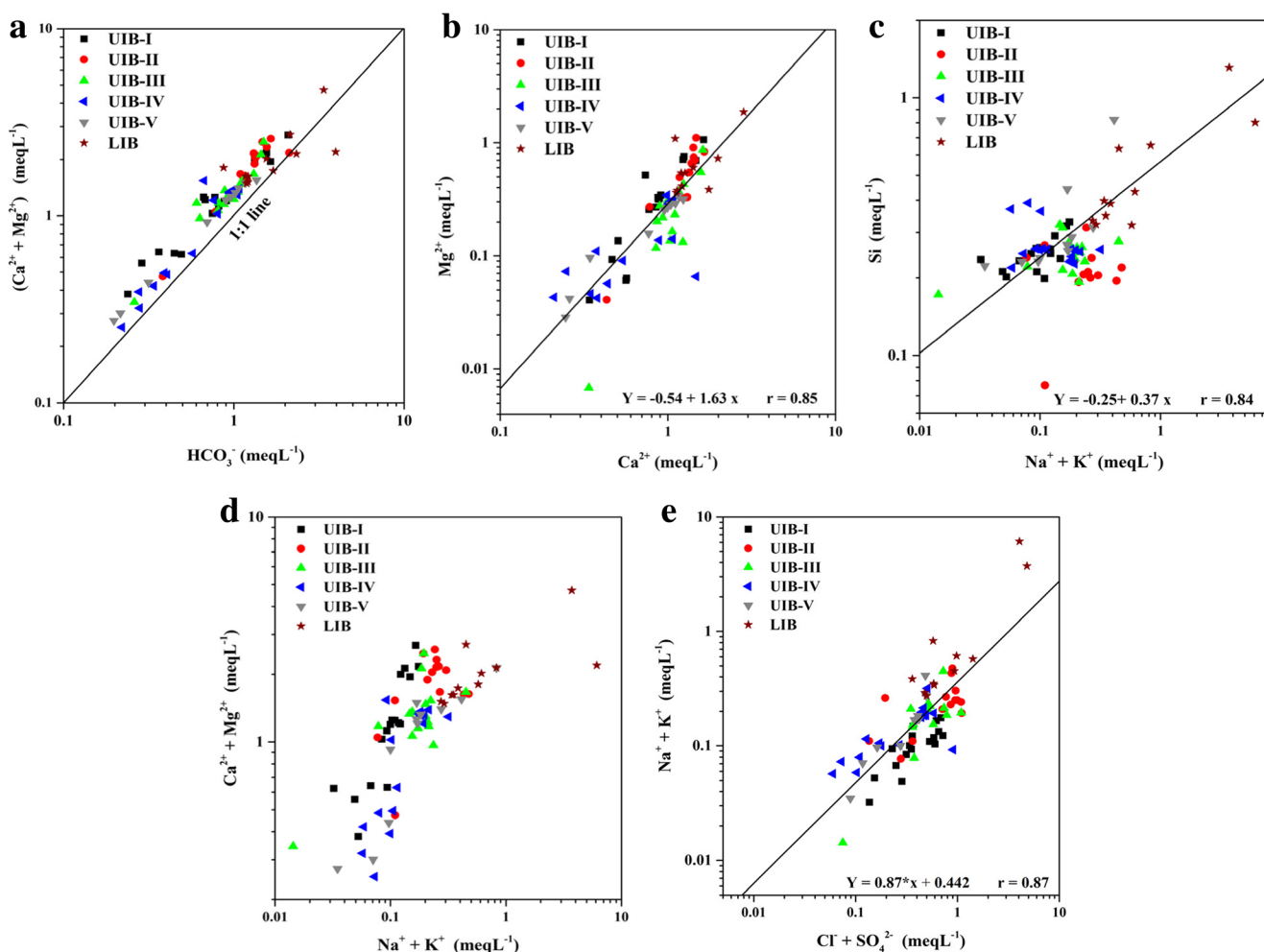


Fig. 5 Scatter diagrams of ions of **a** $\text{Ca}^{2+} + \text{Mg}^{2+}/\text{HCO}_3^-$, **b** $\text{Mg}^{2+}/\text{Ca}^{2+}$, **c** $\text{Si}/\text{Na}^+ + \text{K}^+$, **d** $\text{Ca}^{2+} + \text{Mg}^{2+}/\text{Na}^+ + \text{K}^+$, and **e** $\text{Na}^+ + \text{K}^+/\text{Cl}^- + \text{SO}_4^{2-}$ in surface water of the IRB

basin (Ahmad et al. 1998; Han and Liu 2004; Zhang et al. 2007). For rivers where carbonate is the dominant source, the ratio is high such as 6.7 in the Yarlung Tsangpo River (Qu et al. 2017), 6.0 in part of the Indus River in India (Ahmad et al. 1998), 14.6 in the Upper Han River (Li and Zhang 2008), and 9.72 in the Tigris River (Varol et al. 2013a). In the evaporite-dominated areas with arid environments, $\text{Ca}^{2+} + \text{Mg}^{2+}/\text{Na}^+ + \text{K}^+$ is low, such as 0.6 in the Ejina Basin in northwest China (Si et al. 2009). In this study, UIB-I, UIB-II, UIB-III, UIB-IV, and UIB-V lie in carbonate weathering zones where $\text{Ca}^{2+} + \text{Mg}^{2+}/\text{Na}^+ + \text{K}^+$ ratios were 12.24, 8.55, 8.96, 6.83, and 6.18, respectively. In the LIB, the ratio abruptly decreased to 3.74, affirming that the LIB is influenced more by evaporite dissolution in an arid to semi-arid environment (Habib and Kuper 1998; Habib 2006).

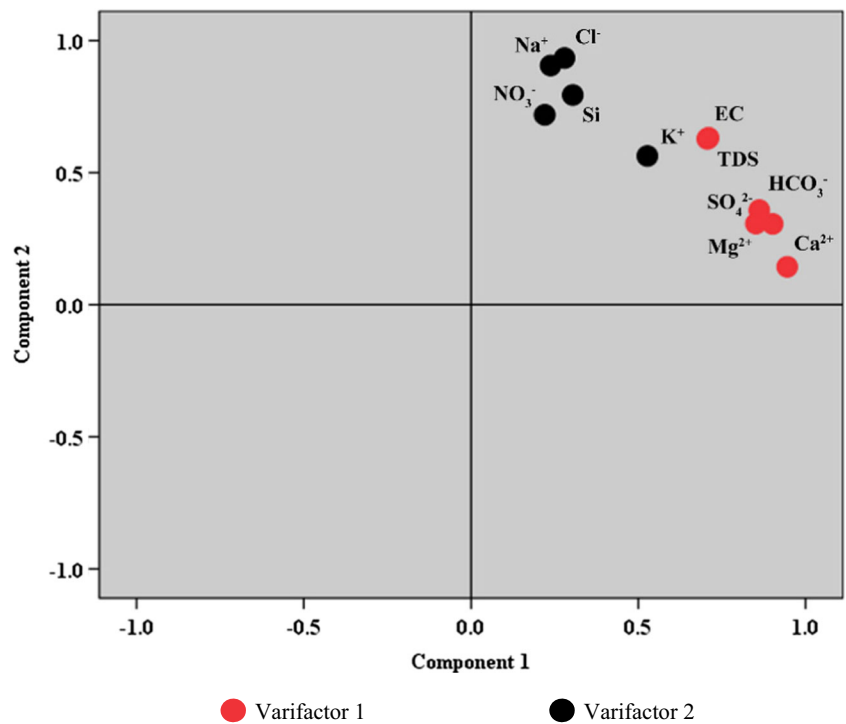
Figure 5e shows that $\text{Na}^+ + \text{K}^+$ was positively correlated with $\text{Cl}^- + \text{SO}_4^{2-}$, suggesting a common source of evaporites for Na^+ , K^+ , Cl^- , and SO_4^{2-} . If halite dissolution is responsible for the Na^+ concentration in any natural water, then the molar ratio of Na^+/Cl^- is approximately 1.0, and if it is > 1.0 , then

the source of Na^+ is other Na-bearing salts (Xiao et al. 2012). In this study, all of the subcatchments have Na^+/Cl^- ratios that are much greater than 1.0 (UIB-I = 1.89, UIB-II = 3.821, UIB-III = 1.82, UIB-IV = 1.91, UIB-V = 2.04, and LIB = 3.55), indicating that Na^+ was released from the weathering of Na-bearing salts, especially in UIB-II and the LIB (Meybeck 1987). In addition, the decreasing order of $\text{Ca}^{2+}/\text{Na}^+$ ratio in different subcatchment is $\text{UIB-I} > \text{UIB-III} > \text{UIB-II} > \text{UIB-IV} > \text{UIB-V} > \text{LIB}$ (i.e., 14.69, 13.23, 12.94, 9.1, 8.47, and 2.62, respectively), revealing the substantial enrichment of Na-bearing salts in the LIB in spite of the dominance of carbonate weathering in the IRB (Table A3).

Principal component/factor analysis

The mechanism governing the chemical compositions of surface water can be assessed by identifying interrelationships and co-variations of parameters (Table A4) using different VFs from PCA/FA (Li and Zhang 2008; Sharma et al. 2016). Factor loading is classified as strong and moderate

Fig. 6 Factor loading plot of the PCA/FA for EC, TDS, major ions, and dissolved silica in the IRB



corresponding to absolute loading values > 0.75 and 0.75–0.5, respectively (Liu et al. 2003).

PCA/FA was firstly applied to the entire normalized data set ($n = 84$) of 11 parameters. The KMO value (0.825) validated the applicability of PCA/FA for the whole data. The analysis evolved two VFs with eigenvalues > 1, explaining about 81.97% of the total variance in the dataset (Fig. 6). The VF1 accounting for 42.97% of the total variance was strongly correlated (> 0.75) with EC, TDS, Ca^{2+} , Mg^{2+} , SO_4^{2-} , and HCO_3^- . The colocation of VF1 components indicate their major contribution to the TDS of the basin and common origin of carbonate rock weathering and sulfate dissolution. Since limestone and gypsum are widely distributed in the soils of the basin, pedogenic activities could also be the potential sources of these components (Singh et al. 2004; Huang et al. 2009; Tripathee et al. 2016a, 2017). The VF2 accounting for 39% of the total variance was strongly correlated with Na^+ , Cl^- , NO_3^- , and Si. The colocation of VF2 components indicated

silicate weathering and breakdown of silicate dominated clay minerals in the basin as their common sources. K^+ is moderately correlated with both VF1 and VF2, with slightly higher loading with VF2, indicating its affinity towards carbonate rocks, since the volcanics and plutonic rocks rick with ultrapotassic garnet and gneisses are widely found in the region (Andrews-Speed and Brookfield 1982; Ahmad et al. 2001).

The results also showed a good agreement with the PCA/FA findings of the subcatchment dataset. For instance, each of the UIB-I, UIB-II, UIB-III, UIB-IV, UIB-V, and LIB have two varifactors explaining the different level of the total variance. In all of the subbasins in the UIB, VF1 had strong loading on Ca^{2+} , Mg^{2+} , Na^+ , SO_4^{2-} , and HCO_3^- , representing the carbonate weathering as a dominant source of dissolved loads in the basin. The VF2 of most of the subbasins in the UIB had strong loading on Cl^- , NO_3^- , K^+ , Na^+ , and Si, indicating the contribution of silicate weathering. The subbasin-wise analysis of PCA/FA, corresponding VFs, variable loadings, and explained variance, are presented in Table A5 and Fig. A4.

Table 3 Classification scheme based on suitability of water for irrigation (Wilcox 1948; Richards 1954)

Parameter	Thresholds	Class	UIB-I	UIB-II	UIB-III	UIB-IV	UIB-V	LIB
Sodium %	< 20	Excellent	17	12	13	15	10	6
	20–40	Good	–	2	1	2	1	3
	40–60	Permissible	–	–	–	–	–	1
	60–80	Doubtful	–	–	–	–	–	1
	> 80	Unsuitable	–	–	–	–	–	–

Drinking and irrigation water quality

The river waters were suitable for drinking purposes based on TDS and ionic contents, as a majority of the parameters were comparable to the global mean and all the parameters fall within the threshold limit of the World Health Organization (Table 1) (Han and Liu 2004; WHO 2011; Varol et al. 2013b; Paudyal et al. 2016).

The high saturation of Na^+ in soil is due to adsorption from water by clay particles, displacing Ca^{2+} and Mg^{2+} , tends to reduce soil permeability, and eventually results in poor internal drainage (Collins and Jenkins 1996; Saleh et al. 1999). The combination of Na^+ with CO_3^{2-} or with Cl^- tends to form more saline soil of both the carbonate and halite types which are not suitable for cropland (Wilcox 1948; Oster 1994). The sodium percentage (Na %) is therefore calculated to assess suitability for irrigation (Eq. 1).

$$\text{Na}\% = \left[\frac{(\text{Na}^+ + \text{K}^+)}{(\text{Ca}^{2+} + \text{Mg}^{2+} + \text{Na}^+ + \text{K}^+)} \right] \times 100 \quad (1)$$

The classification of irrigation waters with respect to sodium percentage by Richards (1954) and Wilcox (1948) is listed in Table 3, where all the samples from UIB-I and a majority of the samples from other subcatchments lie in the “excellent” category, whereas nine samples lie in the “good” category (one each from UIB-III and UIB-V, two each from UIB-II and UIB-IV, and three from the LIB). In the LIB, two samples from major tributaries (Sawan and Deratang) lie in the “permissible” and “doubtful” categories, indicating the low quality of water for irrigation. These tributaries could deteriorate the quality of soil and its agrarian path in the future and could also degrade the agriculture water quality in the downstream direction.

If the waters with high Na^+ and low Ca^{2+} or Mg^{2+} concentration were used for agriculture, the ion exchange in soil may cause saturation of Na^+ and increase the salinity which eventually reduces the osmotic activity of plants and interferes with water and nutrient uptake (Saleh et al. 1999). The Na^+ /alkali hazard, expressed in terms of sodium adsorption ratio (SAR), has been widely used to assess water quality for irrigation purposes (Xiao et al. 2015). Hem (1985) defines SAR as a measure of cation exchange of irrigation water (Eq. 2):

$$\text{SAR} = \text{Na}^+ / \sqrt{(\text{Ca}^{2+} + \text{Mg}^{2+})/2} \quad (2)$$

In the IRB, the mean SAR values in UIB-I, UIB-II, UIB-III, UIB-IV, UIB-V, and the LIB were 0.078 ± 0.019 , 0.12 ± 0.04 , 0.14 ± 0.08 , 0.13 ± 0.05 , 0.18 ± 0.16 , and 0.994 ± 1.58 , respectively. Based on the Bouwer (1978) classification, all of

the water samples belong to the “no problem category” of irrigation water quality, i.e., $\text{SAR} < 6.0$. Water samples from the Deratang tributary in the LIB exhibited higher SAR values of 5.46, which are close to threshold limit, indicating that the water quality of the tributary could be a concern in the future for farmland productivity (Nazeer et al. 2014).

Conclusions

River water in the IRB exhibited an alkaline pH with Ca^{2+} and HCO_3^- as the dominant cation and anion, respectively. The concentrations of major ions in the IRB were more comparable to those of the Yarlung Tsangpo River and the global mean values than those of the other rivers in surrounding regions. The chemical compositions of the river water exhibited distinct spatial patterns from upstream to downstream. Elevated mean concentrations of TDS in the LIB were chiefly ascribed to the arid to semi-arid climatic conditions and relatively higher anthropogenic interference compared to the UIB. The average concentrations of major ions follow the same order of $\text{HCO}_3^- > \text{SO}_4^{2-} > \text{Cl}^- > \text{NO}_3^-$ for anions. However, different orders of cation contents of $\text{Ca}^{2+} > \text{Mg}^{2+} > \text{K}^+ > \text{Na}^+$ and $\text{Ca}^{2+} > \text{Na}^+ > \text{Mg}^{2+} > \text{K}^+$ occurred in the UIB and LIB, respectively, reflecting the diverse nature of geological formation.

Spatial variation patterns and correlation analysis suggested that major ionic concentrations are primarily controlled by the natural processes along with some anthropogenic modifications to NO_3^- . Piper plot showed that chemical facies of river water in the IRB are primarily characterized by the Ca-Mg- HCO_3^- type. The Gibb's plot revealed that most of the water samples in the IRB were dominated by rock weathering, whereas a few samples from the LIB indicated slight evaporation and crystallization processes under the arid to semi-arid climate conditions. The mixing plots illustrated that geochemical compositions of river water in the IRB were dominated by carbonate weathering with the influence of silicate weathering to different degrees and a minor contribution of evaporite dissolution. PCA/FA also indicated that the major sources of dissolved loads in the basin are carbonates followed by silicates in general. In particular, a significant influence of silicate minerals was observed in the LIB, and a higher contribution of evaporites was observed in UIB-II, UIB-III, and the LIB. Ionic ratios illustrated that the major geochemical source is carbonate weathering for Ca^{2+} , Mg^{2+} , and HCO_3^- , silicate weathering in general with additional geogenic and anthropogenic sources in the UIB for Na^+ and K^+ , and Na-bearing salts and evaporites (other than halite) for Cl^- , and SO_4^{2-} .

From the perspective of major ions, the surface water quality of the IRB was found to be within the WHO

permissible limits for drinking purposes except for the high pH. For irrigation, the river water exhibited excellent to good levels in the UIB but excellent to doubtful levels in the LIB. As a result, periodic monitoring of the geochemistry of the IRB is important for the sustainability of riverine ecology and livelihoods of people in the region.

Funding information This research was financially supported by the International Partnership Program of Chinese Academy of Sciences (Grant No. 131C11KYSB20160061), the National Natural Science Foundation of China (Grant No. 41422101), and the Chinese Academy of Sciences-The World Academy of Sciences (CAS-TWAS) President's Fellowship Program

References

- Ahmad T, Khanna PP, Chakrapani GJ, Balakrishnan S (1998) Geochemical characteristics of water and sediment of the Indus river, Trans-Himalaya, India: constraints on weathering and erosion. *J Asian Earth Sci* 16:333–346. [https://doi.org/10.1016/S0743-9547\(98\)00016-6](https://doi.org/10.1016/S0743-9547(98)00016-6)
- Ahmad MN, Fujiwara Y, Paudel LP (2001) Remagnetization of igneous rocks in Gupis area of Kohistan arc, northern Pakistan. *Earth, Planets and Space* 53(5):373–384
- Ali KF, De Boer DH (2007) Spatial patterns and variation of suspended sediment yield in the upper Indus River basin, northern Pakistan. *J Hydrol* 334:368–387
- Andrews-Speed CP, Brookfield ME (1982) Middle Paleozoic to Cenozoic geology and tectonic evolution of the northwestern Himalaya. *Tectonophysics* 82:253–275
- APHA (2005) Standard methods for the examination of water and wastewater. 21st ed. American Public Health Association, Washington DC. Stand Methods Exam Water Wastewater 21st ed Am Public Heal Assoc Washingt DC 1220
- Ashouri H, Hsu K-L, Sorooshian S, Braithwaite DK, Knapp KR, Cecil LD, Nelson BR, Prat OP (2015) PERSIANN-CDR: daily precipitation climate data record from multisatellite observations for hydrological and climate studies. *Bull Am Meteorol Soc* 96:69–83. <https://doi.org/10.1175/BAMS-D-13-00068.1>
- Baig JA, Kazi TG, Arain MB, Afridi HI, Kandhro GA, Sarfraz RA, Jamal MK, Shah AQ (2009) Evaluation of arsenic and other physico-chemical parameters of surface and ground water of Jamshoro, Pakistan. *J Hazard Mater* 166:662–669
- Baloch MS, Awan IU, Hassan G (2006) Growth and yield of rice as affected by transplanting dates and seedlings per hill under high temperature of Dera Ismail Khan, Pakistan. *J Zhejiang Univ B* 7: 572–579
- Barnett TP, Adam JC, Lettenmaier DP (2005) Potential impacts of a warming climate on water availability in snow-dominated regions. *Nature* 438:303–309. <https://doi.org/10.1038/nature04141>
- Battaglin BW, Kendall C, Chang CCY, et al (2001) Isotopic and chemical composition of inorganic and organic water-quality samples from the Mississippi River Basin, 1997–98. *USGS Water Resour Invest Rep* 57
- Bauder TA, Waskom RM, Sutherland PL, et al (2011) Irrigation water quality criteria. *Serv action*; no 0506
- Bouwer H (1978) *Groundwater hydrology*. McGraw-Hill, New York
- Brezonik P, Arnold W (2011) *Water chemistry: an introduction to the chemistry of natural and engineered aquatic systems*. OUP, USA
- Brown GH, Sharp M, Tranter M (1996) Subglacial chemical erosion: seasonal variations in solute provenance, Haut Glacier d'Arolla, Valais, Switzerland. *Ann Glaciol* 22:25–31
- Butz D (1989) The agricultural use of melt water in Hopar settlement, Pakistan. *Ann Glaciol* 13:35–39
- Chen H, Xia Q, Ingrin J (2015) Water content of the Xiaogulihe ultrapotassic volcanic rocks, NE China: implications for the source of the potassium-rich component. *Sci Bull* 60:1468–1470. <https://doi.org/10.1007/s11434-015-0862-4>
- Chen J, Wang F, Meybeck M, et al (2005) Spatial and temporal analysis of water chemistry records (1958–2000) in the Huanghe (Yellow River) basin. Wiley Online Library
- Chen J, Wang F, Xia X, Zhang L (2002) Major element chemistry of the Changjiang (Yangtze River). *Chem Geol* 187:231–255
- Collins R, Jenkins A (1996) The impact of agricultural land use on stream chemistry in the Middle Hills of the Himalayas, Nepal. *J Hydrol* 185:71–86
- Dalai TK, Krishnaswami S, Sarin MM (2002) Major ion chemistry in the headwaters of the Yamuna river system: chemical weathering, its temperature dependence and CO₂ consumption in the Himalaya. *Geochim Cosmochim Acta* 66:3397–3416. [https://doi.org/10.1016/S0016-7037\(02\)00937-7](https://doi.org/10.1016/S0016-7037(02)00937-7)
- Dimri AP, Chevuturi A (2014) Model sensitivity analysis study for west-ern disturbances over the Himalayas. *Meteorog Atmos Phys* 123: 155–180
- Duncan D, Harvey F, Walker M (2007) EPA guidelines: regulatory monitoring and testing. *Water and wastewater sampling*. *Environ Prot Auth J* 3:58
- Gaillardet J, Dupré B, Louvat P, Allègre CJ (1999) Global silicate weathering and CO₂ consumption rates deduced from the chemistry of large rivers. *Chem Geol* 159:3–30. [https://doi.org/10.1016/S0009-2541\(99\)00031-5](https://doi.org/10.1016/S0009-2541(99)00031-5)
- Gburek WJ, Folmar GJ (1999) Flow and chemical contributions to streamflow in an upland watershed: a baseflow survey. *J Hydrol* 217:1–18
- Gibbs RJ (1970) Mechanisms controlling world water chemistry. *Science* 170(80):1088–1090. <https://doi.org/10.1126/science.170.3962.1088>
- Habib Z (2006) Water management and reservoirs in Pakistan. *South Asian J* 11
- Habib Z, Kuper M (1998) Performance assessment of the water regulation and distribution system in the Chishtian sub-division at the main and secondary canal levels. *IWMI*
- Han G, Liu C-Q (2004) Water geochemistry controlled by carbonate dissolution: a study of the river waters draining karst-dominated terrain, Guizhou Province, China. *Chem Geol* 204:1–21. <https://doi.org/10.1016/j.chemgeo.2003.09.009>
- Helena B, Pardo R, Vega M et al (2000) Temporal evolution of ground-water composition in an alluvial aquifer (Pisuerga River, Spain) by principal component analysis. *Water Res* 34:807–816
- Hem JD (1985) *Study and interpretation of the chemical characteristics of natural water*. Department of the Interior, US Geological Survey
- Hewitt K (2005) The Karakoram anomaly? Glacier expansion and the elevation effect, Karakoram Himalaya. *Mt Res Dev* 25:332–340
- Huang X, Sillanpää M, Gjessing ET, Vogt RD (2009) Water quality in the Tibetan Plateau: major ions and trace elements in the headwaters of four major Asian rivers. *Sci Total Environ* 407:6242–6254
- Iqbal HH, Shahid N, Qadir A, Ahmad SR, Sarwar S, Ashraf MR, Arshad HM, Masood N (2017) Hydrological and ichthyological impact assessment of Rasul barrage, river Jhelum, Pakistan. *Polish J Environ Stud* 26:107–114
- Jacobson AD, Blum JD (2000) Ca/Sr and ⁸⁷Sr/⁸⁶Sr geochemistry of disseminated calcite in Himalayan silicate rocks from Nanga Parbat: influence on river-water chemistry. *Geology* 28:463–466
- Jonnalagadda SB, Mhere G (2001) Water quality of the Odzi River in the eastern highlands of Zimbabwe. *Water Res* 35:2371–2376
- Kambole MS (2003) Managing the water quality of the Kafue River. *Phys Chem Earth, Parts A/B/C* 28:1105–1109

- Karim A, Veizer J (2000) Weathering processes in the Indus River basin: implications from riverine carbon, sulfur, oxygen, and strontium isotopes. *Chem Geol* 170:153–177
- Karn SK, Harada H (2001) Surface water pollution in three urban territories of Nepal, India, and Bangladesh. *Environ Manag* 28:483–496
- Kiem A, Ishidaira H, Hapuarachchi HP et al (2008) Future hydroclimatology of the Mekong River basin simulated using the high-resolution Japan Meteorological Agency (JMA) AGCM. *Hydrol Process* 22:1382–1394
- Kimstach VA, Meybeck M (Michel), Baroudy E (1998) A water quality assessment of the former Soviet Union. E & FN Spon
- Li F, Xu Z, Yang H, Liu M (2011) Observed (1961–2009) and projected (2010–2100) climate change over the Yarlung Tsangpo River basin. In: *Water Resource and Environmental Protection (ISWREP)*, 2011 International Symposium on IEEE, pp 2337–2340
- Li S, Zhang Q (2008) Geochemistry of the upper Han River basin, China, 1: spatial distribution of major ion compositions and their controlling factors. *Appl Geochem* 23:3535–3544
- Li X, Ding Y, Yu Z, Mika S, Liu S, Shangguan D, Lu C (2015) An 80-year summer temperature history from the Xiao Dongkemadi ice core in the central Tibetan Plateau and its association with atmospheric circulation. *J Asian Earth Sci* 98:285–295
- Li X, He X, Kang S et al (2016) Diurnal dynamics of minor and trace elements in stream water draining Dongkemadi Glacier on the Tibetan Plateau and its environmental implications. *J Hydrol* 541(Part):1104–1118. <https://doi.org/10.1016/j.jhydrol.2016.08.021>
- Liniger H, Weingartner R, Grosjean M, et al (1998) Mountains of the world: water towers for the 21st century:[a contribution to global freshwater management]. *Mountain Agenda c/o Institute of geography University of Berne*
- Liu C-W, Lin K-H, Kuo Y-M (2003) Application of factor analysis in the assessment of groundwater quality in a blackfoot disease area in Taiwan. *Sci Total Environ* 313:77–89
- Liu H, Li J, Li X, Zheng Y, Feng S, Jiang G (2015) Mitigating greenhouse gas emissions through replacement of chemical fertilizer with organic manure in a temperate farmland. *Sci Bull* 60:598–606. <https://doi.org/10.1007/s11434-014-0679-6>
- Liu Z, Ostrenga D, Teng W, Kempler S (2012) Tropical rainfall measuring mission (TRMM) precipitation data and services for research and applications. *Bull Am Meteorol Soc* 93:1317–1325
- Loveland TR, Reed BC, Brown JF, Ohlen DO, Zhu Z, Yang L, Merchant JW (2000) Development of a global land cover characteristics database and IGBP DISCover from 1 km AVHRR data. *Int J Remote Sens* 21:1303–1330
- Lutz AF, Immerzeel WW, Kraaijenbrink PDA, Shrestha AB, Bierkens MFP (2016) Climate change impacts on the upper Indus hydrology: sources, shifts and extremes. *PLoS One* 11:e0165630. <https://doi.org/10.1371/journal.pone.0165630>
- Manoj K, Ghosh S, Padhy PK (2013) Characterization and classification of hydrochemistry using multivariate graphical and hydrostatistical techniques. *Res J Chem Sci ISSN* 2231:606X
- Meybeck M (2003) Global occurrence of major elements in rivers. *Treatise Geochem* 5:207–223
- Meybeck M (1987) Global chemical weathering of surficial rocks estimated from river dissolved loads. *Am J Sci* 287:401–428. <https://doi.org/10.2475/ajs.287.5.401>
- Moon S, Huh Y, Zaitsev A (2009) Hydrochemistry of the Amur River: weathering in a northern temperate basin. *Aquat Geochem* 15:497–527. <https://doi.org/10.1007/s10498-009-9063-6>
- Nadeem Faisal (2015) Annual report on 2015 Pakistan's Monsoon Rainfall
- Nazeer S, Hashmi MZ, Malik RN (2014) Heavy metals distribution, risk assessment and water quality characterization by water quality index of the river Soan, Pakistan. *Ecol Indic* 43:262–270
- Oster JD (1994) Irrigation with poor quality water. *Agric Water Manag* 25:271–297
- Pande K, Sarin MM, Trivedi JR, Krishnaswami S, Sharma KK (1994) The Indus river system (India-Pakistan): major-ion chemistry, uranium and strontium isotopes. *Chem Geol* 116:245–259
- Pant RR, Zhang F, Rehman FU et al (2018) Spatiotemporal variations of hydrogeochemistry and its controlling factors in the Gandaki River Basin, Central Himalaya Nepal. *Sci Total Environ* 622:770–782
- Patz JA, Campbell-Lendrum D, Holloway T, Foley JA (2005) Impact of regional climate change on human health. *Nature* 438:310–317. <https://doi.org/10.1038/nature04188>
- Paudyal R, Kang S, Sharma CM, Tripathee L, Huang J, Rupakheti D, Sillanpää M (2016) Major ions and trace elements of two selected rivers near Everest region, southern Himalayas, Nepal. *Environ Earth Sci* 75:1–11. <https://doi.org/10.1007/s12665-015-4811-y>
- Pekey H, Karakaş D, Bakoglu M (2004) Source apportionment of trace metals in surface waters of a polluted stream using multivariate statistical analyses. *Mar Pollut Bull* 49:809–818
- Piper AM (1944) A graphic procedure in the geochemical interpretation of water analyses. *EOS Trans Am Geophys Union* 25:914–928
- Qadir A, Malik RN, Husain SZ (2008) Spatio-temporal variations in water quality of Nullah Aik-tributary of the river Chenab, Pakistan. *Environ Monit Assess* 140:43–59. <https://doi.org/10.1007/s10661-007-9846-4>
- Qu B, Zhang Y, Kang S, Sillanpää M (2017) Water chemistry of the southern Tibetan Plateau: an assessment of the Yarlung Tsangpo river basin. *Environ Earth Sci* 76:74. <https://doi.org/10.1007/s12665-017-6393-3>
- Raymo ME, Ruddiman WF (1992) Tectonic forcing of late Cenozoic climate. *Nature* 359:117–122
- Reynolds RC, Johnson NM (1972) Chemical weathering in the temperate glacial environment of the northern Cascade Mountains. *Geochim Cosmochim Acta* 36:537–554
- Richards LA (1954) Diagnosis and improvement of saline and alkali soils. LWW
- Richardson M, Hausfather Z, Nuccitelli DA, Rice K, Abraham JP (2015) Misdiagnosis of earth climate sensitivity based on energy balance model results. *Sci Bull* 60:1370–1377. <https://doi.org/10.1007/s11434-015-0806-z>
- Saleh A, Al-Ruwaih F, Shehata M (1999) Hydrogeochemical processes operating within the main aquifers of Kuwait. *J Arid Environ* 42:195–209
- Selemeni JR, Zhang J, Muzuka ANN, Njau KN, Zhang G, Maggid A, Mzuza MK, Jin J, Pradhan S (2017) Seasonal water chemistry variability in the Pangani River basin, Tanzania. *Environ Sci Pollut Res* 24:26092–26110. <https://doi.org/10.1007/s11356-017-0221-x>
- Shammi M, Rahman MM, Islam MA, Bodrud-Doza M, Zahid A, Akter Y, Quaiyum S, Kurasaki M (2017) Spatio-temporal assessment and trend analysis of surface water salinity in the coastal region of Bangladesh. *Environ Sci Pollut Res* 24:14273–14290. <https://doi.org/10.1007/s11356-017-8976-7>
- Sharma A, Singh AK, Kumar K (2012) Environmental geochemistry and quality assessment of surface and subsurface water of Mahi River basin, western India. *Environ Earth Sci* 65:1231–1250
- Sharma S, Roy A, Agrawal M (2016) Spatial variations in water quality of river Ganga with respect to land uses in Varanasi. *Environ Sci Pollut Res* 23:21872–21882. <https://doi.org/10.1007/s11356-016-7411-9>
- Si J, Qi F, Xiaohu W et al (2009) Major ion chemistry of groundwater in the extreme arid region northwest China. *Environ Geol* 57:1079–1087
- Singh KP, Malik A, Mohan D, Sinha S (2004) Multivariate statistical techniques for the evaluation of spatial and temporal variations in water quality of Gomti River (India)—a case study. *Water Res* 38:3980–3992
- Stallard RF, Edmond JM (1987) Geochemistry of the Amazon: 3. Weathering chemistry and limits to dissolved inputs. *J Geophys Res* 92:8293. <https://doi.org/10.1029/JC092iC08p08293>

- Stumm W, Morgan JJ (2012) *Aquatic chemistry: chemical equilibria and rates in natural waters*. John Wiley & Sons, Hoboken
- Subramanian V (1979) Chemical and suspended-sediment characteristics of rivers of India. *J Hydrol* 44:37–55
- Sun B, Zhang L, Yang L, Zhang F, Norse D, Zhu Z (2012) Agricultural non-point source pollution in China: causes and mitigation measures. *Ambio* 41:370–379
- Tahir AA, Adamowski JF, Chevallier P, Haq AU, Terzago S (2016) Comparative assessment of spatiotemporal snow cover changes and hydrological behavior of the Gilgit, Astore and Hunza River basins (Hindukush–Karakoram–Himalaya region, Pakistan). *Meteorog Atmos Phys* 128:793–811
- Tahir AA, Chevallier P, Arnaud Y, Neppel L, Ahmad B (2011) Modeling snowmelt-runoff under climate scenarios in the Hunza River basin, Karakoram Range, Northern Pakistan. *J Hydrol* 409:104–117
- Thomas J, Joseph S, Thrivikramji KP, Manjusree TM, Arunkumar KS (2014) Seasonal variation in major ion chemistry of a tropical mountain river, the southern Western Ghats, Kerala, India. *Environ Earth Sci* 71:2333–2351
- Tian Y, Yu C, Zha X, Wu J, Gao X, Feng C, Luo K (2016) Distribution and potential health risks of arsenic, selenium, and fluorine in natural waters in Tibet, China. *Water* 8:568
- Tripathee L, Kang S, Huang J, Sillanpää M, Sharma CM, Lüthi ZL, Guo J, Paudyal R (2014) Ionic composition of wet precipitation over the southern slope of central Himalayas, Nepal. *Environ Sci Pollut Res* 21:2677–2687
- Tripathee L, Kang S, Rupakheti D, Cong Z, Zhang Q, Huang J (2017) Chemical characteristics of soluble aerosols over the central Himalayas: insights into spatiotemporal variations and sources. *Environ Sci Pollut Res* 24:24454–24472
- Tripathee L, Kang S, Rupakheti D, Zhang Q, Bajracharya RM, Sharma CM, Huang J, Gyawali A, Paudyal R, Sillanpää M (2016a) Spatial distribution, sources and risk assessment of potentially toxic trace elements and rare earth elements in soils of the Langtang Himalaya, Nepal. *Environ Earth Sci* 75:1332
- Tripathee L, Kang S, Sharma CM, Rupakheti D, Paudyal R, Huang J, Sillanpää M (2016b) Preliminary health risk assessment of potentially toxic metals in surface water of the Himalayan rivers, Nepal. *Bull Environ Contam Toxicol* 97:855–862. <https://doi.org/10.1007/s00128-016-1945-x>
- Varol M, Gökot B, Bekleyen A (2013a) Dissolved heavy metals in the Tigris River (Turkey): spatial and temporal variations. *Environ Sci Pollut Res* 20:6096–6108
- Varol M, Gökot B, Bekleyen A, Şen B (2013b) Geochemistry of the Tigris River basin, Turkey: spatial and seasonal variations of major ion compositions and their controlling factors. *Quat Int* 304:22–32. <https://doi.org/10.1016/j.quaint.2012.12.043>
- Vörösmarty CJ, McIntyre PB, Gessner MO et al (2010) Global threats to human water security and river biodiversity. *Nature* 467:555–561
- Wang G, Zeng C, Zhang F, Zhang Y, Scott CA, Yan X (2017) Traffic-related trace elements in soils along six highway segments on the Tibetan plateau: influence factors and spatial variation. *Sci Total Environ* 581–582:811–821. <https://doi.org/10.1016/j.scitotenv.2017.01.018>
- Wang J, Yan W, Jia X (2006) Modeling the export of point sources of nutrients from the Yangtze River basin and discussing countermeasures. *Acta Sci Circumst* 26:658–666
- WHO (2011) *Guidelines for drinking-water quality*. Geneva: world health organization
- Wilcox LV (1948) *The quality of water for irrigation use*. United States Department of Agriculture, Economic Research Service
- Wu L, Long T, Liu X, Guo J (2012) Impacts of climate and land-use changes on the migration of non-point source nitrogen and phosphorus during rainfall-runoff in the Jialing River watershed, China. *J Hydrol* 475:26–41
- Xiao J, Jin Z-D, Ding H et al (2012) Geochemistry and solute sources of surface waters of the Tarim River Basin in the extreme arid region, NW Tibetan Plateau. *J Asian Earth Sci* 54:162–173
- Xiao J, Jin ZD, Wang J, Zhang F (2015) Hydrochemical characteristics, controlling factors and solute sources of groundwater within the Tarim River Basin in the extreme arid region, NW Tibetan Plateau. *Quat Int* 380:237–246
- Young GJ, Hewitt K (1990) Hydrology research in the upper Indus basin, Karakoram Himalaya, Pakistan. *Hydrol Mt Areas. IAHS Publ* 190: 139–152
- Zhang Q, Xu C-Y, Yang T (2009) Variability of water resource in the Yellow River basin of past 50 years, China. *Water Resour Manag* 23:1157–1170
- Zhang S-R, Lu XX, Higgitt DL, Chen CTA, Sun HG, Han JT (2007) Water chemistry of the Zhujiang (Pearl River): natural processes and anthropogenic influences. *J Geophys Res* 112:F01011. <https://doi.org/10.1029/2006JF000493>